nature communications

Article

https://doi.org/10.1038/s41467-024-54939-y

Metamaterial-based injection molding for the cost-effective production of whole cuts

Received: 17 March 2024

Accepted: 22 November 2024

Published online: 30 December 2024

Check for updates

Mohammad Ghosheh[1,2], Avner Ehrlich[1,2], Amit Fischer[3], Laura Pasitka[1], Merav Cohen[1,2,4] & Yaakov Nahmias[1,2,4]

The escalating global demand for meat products has intensified ecological concerns, underscoring the need for sustainable meat alternatives. Although current methods effectively imitate ground meat, mimicking whole cuts, which constitute 54% of the global market, remains challenging due to the lack of scalable technology. Injection molding is a massively scalable manufacturing technology developed for the polymer industry. Here, we introduce two injectable metamaterials: a thermally irreversible fat composite we named proteoleogel, and a multi-scaled meat analog produced by low-temperature extrusion. Viscoelastic screening of plant proteins identifies mung bean for its ability to stabilize complex oleogel structures, mimicking the mechanics of adipose tissue. Mechanical analysis reveals that low-temperature extrusion produces microscale isotropic fibers and mesoscale anisotropic structures mimicking muscle and fascia. These metamaterials can be injection-molded into various whole cuts, from chops to T-bones. Blinded taste tests indicate a 43% preference for our plant-based steak analog. Moreover, technical economic analysis shows injection molding is more cost-effective than 3D printing, costing $9/kg compared to $38/kg. This research represents a step in sustainable food production, offering cost-effective and scalable solutions for the entire meat market.

The global demand for meat is projected to increase by 50% over the next two decades, driven by population growth and urbanization[1,2]. A recent report by the Food and Agriculture Organization determines that animal farming contributes 14.5% of global greenhouse gas emissions, impacts animal diversity, and consumes 20% of the global freshwater supply[3]. These growing environmental demands spurred research into alternative protein sources. Current approaches range from plant protein to fungi and cell-based protein production termed cultivated meat[4–11]. Current estimates suggest the shift to plant-based meat would produce 96-98% less greenhouse gas emissions and use 67–97% less freshwater than traditional agriculture[12].

The global meat market stood at $1378 billion in 2023, representing a volume of over 350×10^9 kg of meat products annually[13]. Current approaches successfully reproduce the texture of ground meat products[14,15], such as hamburgers and meatballs using textured vegetable protein[16] or tissue engineering[17,18]. However, the manufacturing of complex whole cuts, which constitute about 54% of the market is limited to 3D printing[19,20]. 3D bioprinting of cells was originally developed by Wilson and Boland in 2003 and taken to its resolution limit by Nahmias and colleagues[21–23]. 3D printing produces multiscale materials slowly, depositing one fiber at a time through additive manufacturing. This process is thus inherently limited to the rate of deposition of fibers with a diameter ranging from 0.1-1 mm, requiring high-resolution motors and technical expertise that further limit process scalability[24,25]. In fact, recent advances in 3D printing of whole cuts reached a production rate of 6 kg/h at a cost of $20 per kg of printed steak[26].

[1]Alexander Grass Center for Bioengineering, The Hebrew University of Jerusalem, Jerusalem, Israel. [2]The Rachel and Selim Benin School of Computer Science and Engineering, The Hebrew University of Jerusalem, Jerusalem, Israel. [3]Department of Biological Chemistry, Institute of Chemistry, The Hebrew University of Jerusalem, Jerusalem, Israel. [4]Department of Genetics, The Hebrew University of Jerusalem, Jerusalem, Israel. e-mail: yaakov.nahmias@mail.huji.ac.il

Injection molding is a high-capacity plastic manufacturing technology developed by James Watson Hendy in the 1940s[27]. This $262 billion industry utilizes low-temperature extrusion to inject molten polymers into molds, creating complex multi-material products[28]. The application of injection molding to meat manufacturing would double the total addressable market of meat alternatives.

The challenge lies in the multiscale nature of meat. Meat is a crosscut of overlocking muscles 1–5 cm in diameter. Muscles are composed of parallel fascicles and fibers that are 1 and 0.1 mm in diameter[29,30]. Small mesoscale isotropy contributes to tangential bite strength, an important texture[30]. Animal fat is a similarly complex connective tissue that can be chemically described as a protein hydrogel permeated with lipid droplets. While plant-based oils (i.e., coconut oil) rapidly melt during cooking, animal fat binds oil droplets during cooking while creating stable connections between muscle and bone elements in the meat[31,32].

Metamaterials are one technology capable of generating complex multiscale products. For example, silica aerogels, form a multiscale silica mesh with low thermal connectivity and high surface area utilized in spacecraft and reaction engineering[33]. Here we present two injectable metamaterials optimized for the efficient and cost-effective production of meat analogs.

In this work we describe the low-temperature extrusion of textured plant protein, creating a multiscaled meat analog that replicates the complex mechanical properties of meat. We also describe the production of a plant-protein stabilized oleogel, which we name proteoleogel, capable of retaining lipid droplets during cooking while creating stable connections between muscle and bone elements in the meat. We demonstrate that the metamaterials can be efficiently injected into a mold rapidly creating complex chops and steaks. Injection-molded steaks and chops are assessed in a blinded sensory study. Finally, we carry out a detailed technical economic analysis demonstrating the cost-efficacy of injection molding over 3D printing. This work addresses both the scalability and cost challenges associated with 3D printing, offering a distinctive, mass-production solution for meat alternatives.

Results

Injection molding of whole meat cuts: process and economics

Injection molding is a high-capacity manufacturing process used to produce plastics. To adjust the process for whole-cut manufacturing we 3D scanned an entrecote steak and printed a bottom mold in its exact contours (Fig. 1A). Bone cement was molded to the shape of the entrecote bone (Supplementary Fig. S1A–C), cured, and placed into the steak mold. A top mold, with multiple cavities shaped to the contours of individual muscles, was compressed on the bottom mold. Extruded protein was then injected into the closed cavities at 70 °C and frozen in place to allow top mold removal. The process then lowered a third mold, through which proteoleogel was injected at room temperature flowing into the spaces left between muscles by top mold removal. Surface cooling allowed the product to be easily removed from the bottom mold (Fig. 1B), starting the process again (Fig. 1A, B).

To evaluate the economic aspects of manufacturing using injection molding compared to 3D printing we analyzed the cost efficacy of both manufacturing processes. We evaluated production costs at 5 and 125 tons, including machine, tooling, and labor expenses (Fig. 1C). The cost of manufacturing 5 tons of product using injection molding was $11.9 per kg, compared to $5 per kg for 3D printing. However, at the 125ton scale, the cost for injection molding decreased to $1.6 per kg, about 68% less than 3D printing at an equivalent volume as fixed costs, such as mold design (i.e., tooling), were spread over more units. In contrast, 3D printing scaleup is primarily dependent on parallelization, limiting the reduction in fixed costs[34] (Fig. 1C). The breakeven point for injection molding was 25 ton (Fig. 1D; Supplementary Fig. S1D), emphasizing the potential of this scalable technology in large scale meat manufacturing.

Development of Low-Temperature Meat Analog (LTMA)

Muscle bundles exhibit a complex multiscale architecture, of overlapping macroscopic fascicles that are 1 mm in diameter, which are subdivided into fibers about 0.2 mm in diameter (Fig. 2A, D, F)[29,30]. Muscle mesoscale isotropy plays an important role in its mechanical properties reflected in its tangential bite strength[35]. High moisture extrusion is a manufacturing process in which protein concentrate is denatured at 130 to 170 °C and sheared in high pressure to align and crosslink nanoscale protein fibers (Fig. 2B). Slug flow cooling produces protein layers that range from 0.4 to 4 mm in thickness, creating high moisture meat analogs (HMMA)[36,37]. Low-temperature extrusion is an alternative process that uses plant protein that was already textured using dry extrusion. Pellets, rather than powder, are mixed with an emulsion and fed into a single-screw extrusion at temperatures of 80–95 °C allowing the fibers to gel (Fig. 2C). The product is then compressed in a cooling step, creating a multiscaled metamaterial. The gelled fibers between the screw blades are compressed together, providing a fascicle-like texture 5–12 mm in diameter (Fig. 2D–G). Textured proteins trapped by the gel are oriented by flow to bundles of microscale fibers between 0.5–1 mm in diameter, emulating muscle fibers, thus creating a low-temperature meat analog (LTMA, Fig. 2D–G).

Optical microscopy of beef, HMMA, and LTMA demonstrated fascicle-like structures in beef and LTMA. At the same time, HMMA showed sheet-like organization (Fig. 2D). Scanning electron microscopy (SEM) was used to analyze the fine structure of beef, HMMA, and LTMA (Fig. 2E). The microscopic analysis of beef muscle revealed hundreds of closely packed beef muscle fibers 170 ± 30 μm in diameter interconnected by extracellular mesh as optically observed fascicles that are 0.5 to 1.5 mm in diameter (Fig. 2F). Electron and optical microscopy of HMMA shows a different organization, with semi-diffuse layers distributed from 0.4 to 3.5 mm in thickness overlayed on each other (Fig. 2D–F). The quantification of the fiber diameter in SEM images of LTMA revealed a multi-scaled organization like a beef muscle, with interconnected fibers that are 200 ± 50 μm in diameter, not different from muscle ($p > 0.05$), and optical microscopy observed fascicle-like structures that are 1.2 ± 0.3 mm in diameter (Fig. 2F). Visual inspection showed different gross structural organization between LTMA and HMMA, revealing bundle like structures in LTMA about 5 mm in size (Fig. 2G). We next sought to test whether the multi-scaled organization of LTMA affected its mechanical properties.

To compare the mechanical properties of HMMA and LTMA to beef muscle we carried out stress analysis in both longitudinal (i.e., parallel to extrusion direction) and perpendicular direction on the extruded product, before injection molding (Fig. 2H–O). The nutritional profile of lean beef, LTMA, and HMMA shows similar protein and fat content of the extruded product that was mechanically analyzed (Supplementary Table S13).

Force-displacement curves of the longitudinal section showed similar force generation of beef muscle to LTMA (Fig. 2H). Maximal load, a proxy for chew resistance, showed 71% lower resistance in HMMA compared to beef ($p < 0.001$), while the maximal load of LTMA was not significantly different from beef (Fig. 2I). The elastic strain energy, is indicative of textural resilience and bite feel showed similar stress development between LTMA and beef (Fig. 2J). Product toughness modulus was 85% lower in HMMA compared to beef ($p < 0.001$), while the toughness of LTMA was not significantly different from beef (Fig. 2K).

Force-displacement curves of perpendicular sections are important for discerning textures[38] and the mouth feel of beef[39,40]. Both force-displacement and stress-strain curves show similar force generation of beef muscle to LTMA in the perpendicular section (Fig. 2L).

Analysis showed that the maximal load of both HMMA and LTMA in the perpendicular section was about 15% lower than beef ($p < 0.001$). However, the elastic strain energy of LTMA was not significantly different from beef (Fig. 2M), while HMMA showed 83% lower resistance ($p < 0.01$). Product toughness modulus was 88% lower in HMMA compared to beef ($p < 0.001$), while the toughness of LTMA was not significantly different from beef (Fig. 2N, O). This assessment demonstrates similar chewiness and resilience of LTMA and beef, contrasting with a significantly lower resistance of HMMA resulting in a more gummy texture. While biting LTMA in the perpendicular direction would offer more resistance than HMMA, it would still be softer than beef.

Development of protein-stabilized oleogels

Oleogels are semi-solid materials formed by the dispersion of a structuring agent with liquid oil, resulting in high-viscosity, gel-like material, that replaces trans fats in food applications (Fig. 3A)[31,41]. While oleogels become liquid at high temperatures, the protein matrix in animal fats denatures during cooking binding moisture, muscle, and bone[35].

As recent work suggested that plant proteins can increase the viscosity of oleogels[32,42], we sought to identify plant proteins capable of creating irreversible gel during cooking, emulating the function of animal fats (Fig. 3A). Protein-containing oleogels were produced by high shear emulsification and compared to minced animal fat and

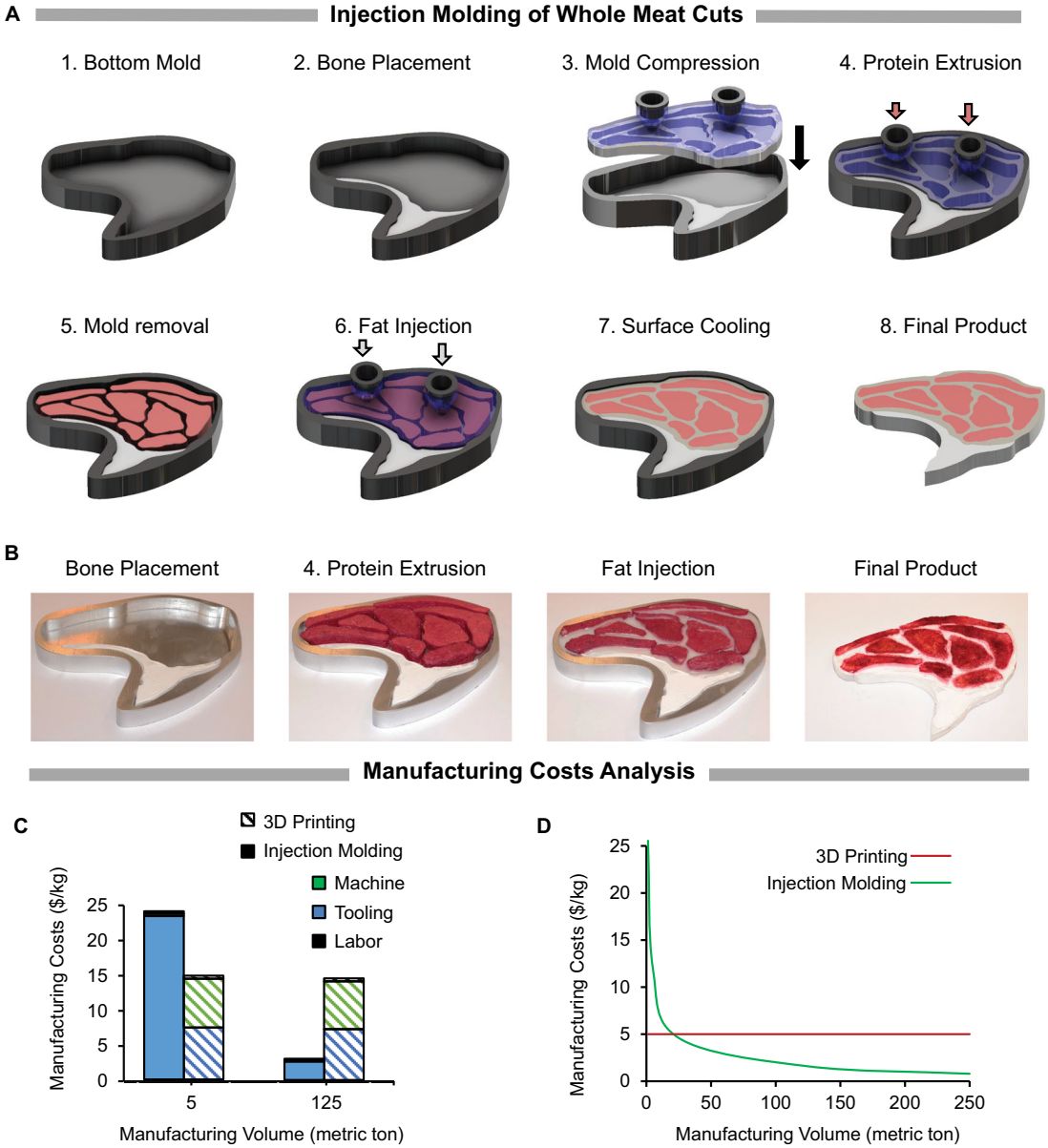

Fig. 1 | Design and economic analysis of injection molding in whole meat cut manufacturing. A Computer-aided design (CAD) process depicting the sequential injection molding process phases, demonstrating the reproduction of entrecote steak analog. **B** Photographs depicting the stages of the injection molding process used to reproduce a meat analog of an entrecote steak. Dyes were used for clarity. **C** A comprehensive analysis of machine, tooling, and labor expenses of 3D printing compared to injection molding. The evaluation was conducted for lab-scale manufacturing of 5 tons and pilot-scale production of 125 tons per month, elucidating manufacturing costs ($/kg). At 5 tons, injection molding incurs costs of 11.9 $/kg, while 3D printing entails expenses of 5 $/kg, resulting in a substantial 136% cost increase. In contrast, at 125 tons, injection molding's cost decreases to 1.6 $/kg, compared to 3D printing's cost of 5 $/kg, demonstrating a notable 68% cost reduction. These findings underscore a 3-fold cost advantage of injection molding at 125 tons. **D** Comprehensive cost comparison underscores injection molding's economic edge over 3D printing, highlighting cost trends and efficiency, with a breakeven point at 25 tons per month, showcasing cost-effectiveness in even small-scale manufacturing.

https://doi.org/10.1038/s41467-024-54939-y

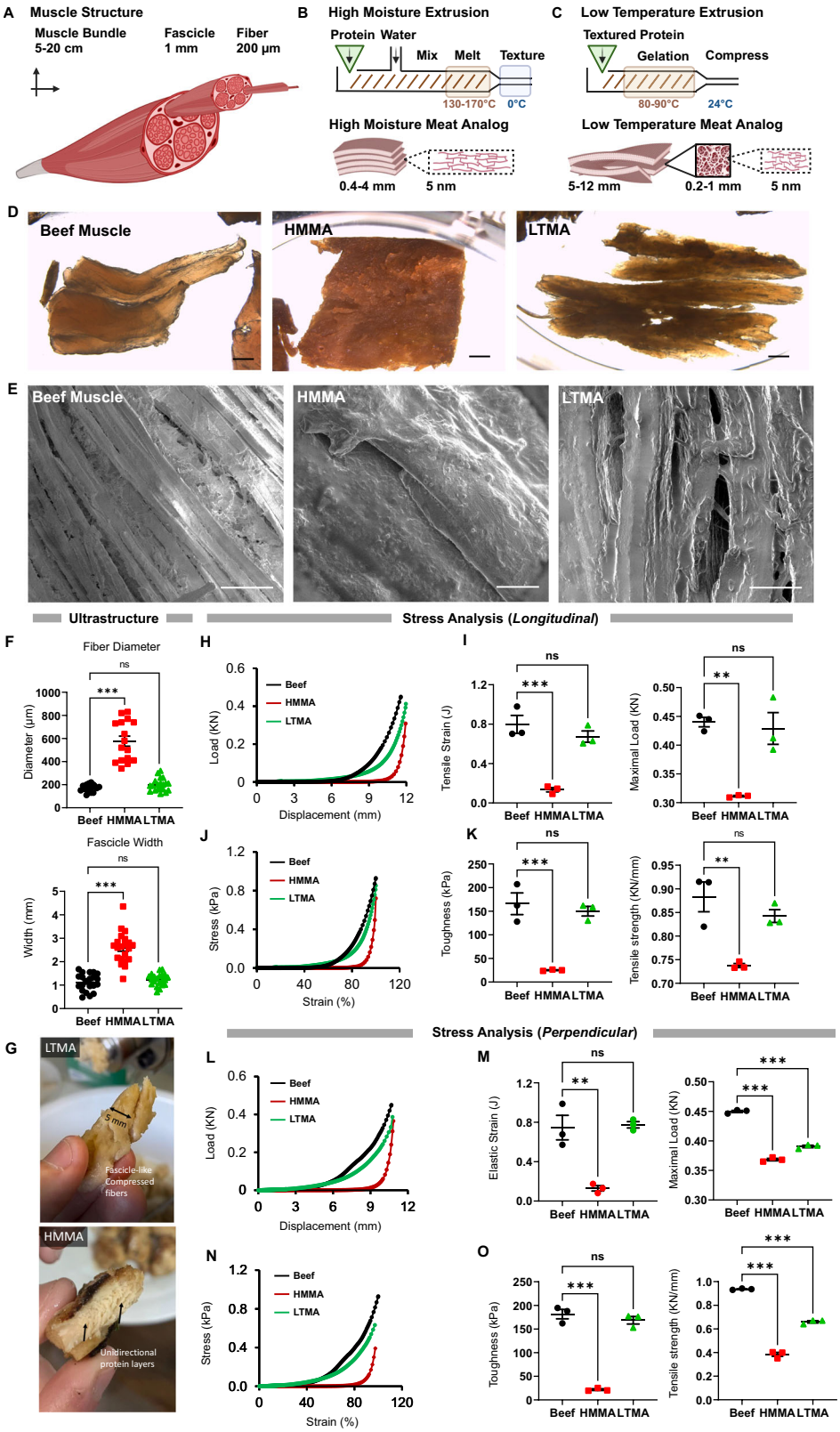

standard oleogel composed of water, vegetable oil, and emulsifier. Chickpea, potato, soybean, pea, mung bean, lentil, and rice proteins were used at 2.5% weight per volume ("Methods"). Morphological inspection of the materials at room temperature showed the oleogels formed with mung bean, soybean, and pea proteins exhibiting structural integrity reminiscent of animal fats (Fig. 3B).

Rheological analysis was carried out on a modular advanced rheometry system (MARS) quantifying the storage (G') and loss (G") modulus of each material (Fig. 3C, D). Our analysis showed significant differences between the proteins examined. Potato and rice proteins showed G' and G" that were different, but only marginally higher than oleogel, possibly due to the high starch content of potato and rice

https://doi.org/10.1038/s41467-024-54939-y

Fig. 2 | Structural and mechanical properties of LTMA metamaterial produced by low-temperature extrusion. A, Schematic depicting the complex multiscale architecture of muscle bundles. The multiscale structure defines muscle mesoscale isotropy, generating the tangential bite strength of meat. **B** Schematic depicting a high moisture extrusion process resulting in the formation of high-moisture meat analogs (HMMA). **C** Schematic depicting our low-temperature extrusion process resulting in the production a multiscale structure with muscle-like mesoscale isotropy termed low-temperature meat analogs (LTMA). **D** Optical stereo microscopy of beef, HMMA, and LTMA revealed fascicle-like structures in beef and LTMA, while HMMA exhibited a sheet-like organization. Scale bar = 1 mm **E** Scanning electron micrographs of farmed beef, HMMA, and LTMA showing fiber ultrastructure. Scale bar = 250 μm. **F** Quantification of fiber diameter in SEM images of LTMA. (ns $P > 0.05$, ***$P < 0.001$; $n = 9$). **G** Visual assessments of cooked HMMA and LTMA reveal distinct gross structural organizations. **H** Force-displacement analysis across the longitudinal fibers (force-generating axis) of farmed beef, HMMA, and LTMA. Force generation of LTMA was comparable to farmed beef. **I** Comparative analysis of elastic strain energy and maximal load across the longitudinal fibers of farmed beef, HMMA, and LTMA. (ns $P > 0.05$, ** $P \leq 0.01$, *** $P \leq 0.001$; $n = 3$). **J** Representative stress-strain curves elucidating the biomechanical behavior of farmed beef, HMMA, and LTMA across their longitudinal fibers. **K** Quantitative assessment of toughness modulus and ultimate tensile strength. (ns $P > 0.05$, *** $P \leq 0.001$; $n = 3$). **L** Force–displacement curves derived from compression tests across the perpendicular fibers of farmed beef, HMMA, and LTMA. Force generation of LTMA was comparable to farmed beef. **M** Analysis of elastic strain energy data reveals HMMA was 17% of beef, while LTMA was not significantly different from beef. (ns $P > 0.05$, ** $P \leq 0.01$, *** $P \leq 0.001$; $n = 3$). **N** Stress-strain curves of farmed beef, HMMA, and LTMA. **O** Analysis of toughness modulus of farmed beef, HMMA, and LTMA. Tensile strength assessment captures the resilience of materials under biting and chewing forces in mastication. (ns $P > 0.05$, *** $P \leq 0.001$; $n = 3$). All n values represent the number of experimental repeats. Error bars indicate ± s.e.m. Figure 2a–c was created in BioRender. Cohen, M. (2023) https://BioRender.com/v89n608.

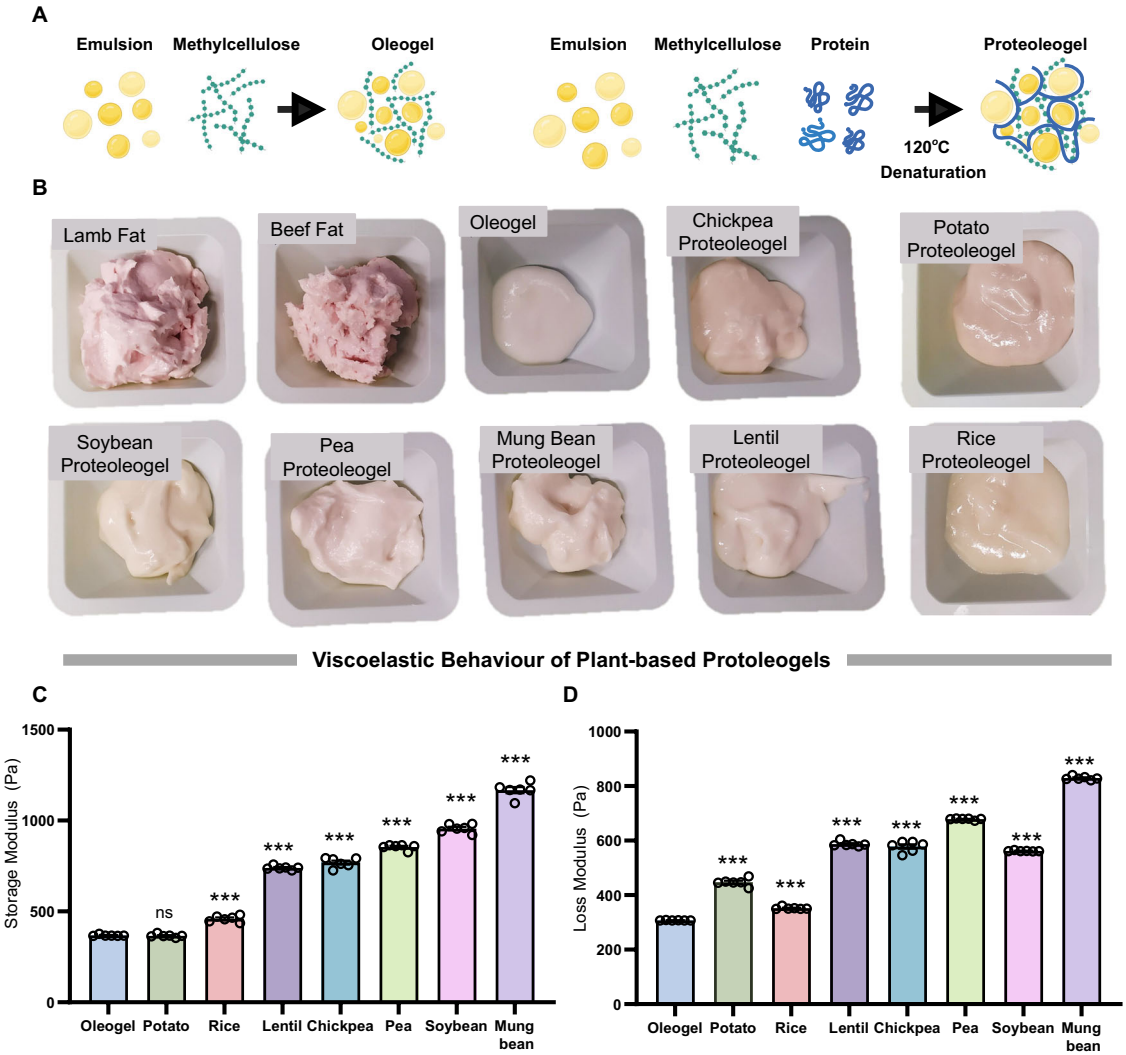

Fig. 3 | Development of plant-based proteoleogel (PToG) metamaterial. **A** Scheme illustrating the composition of standard oleogel, and a protein-stabilized thermally irreversible metamaterial we termed proteoleogel (PToG). **B** Morphological images showcase raw minced lamb fat, beef fat, standard oleogel, and proteoleogels derived from isolates of chickpea, potato, soybean, pea, mung bean, lentil, and rice. Visual inspection showed that mung bean, soybean, and pea proteins showed higher structural consistency than other plant proteins. **C** Rheological investigation of proteoleogels derived from isolates of chickpea, potato, soybean, pea, mung bean, lentil, and rice. Storage modulus (G′) values are shown in (**C**), and loss modulus (G″) values in (**D**). Storage Modulus (G′) of mung bean, and soybean was 160% to 214% higher than standard oleogel ($p < 0.001$, $n = 5$). The loss Modulus (G″) of Mung bean was 168% higher than standard oleogel ($p < 0.001$, $n = 5$), indicating superior structural and rheological properties. (ns $P > 0.05$, *** $P \leq 0.001$; $n = 3$). Significance was determined using a one-way ANOVA with Dunnett correction. All n values represent the number of experimental repeats. Error bars indicate ± s.e.m. Figure 3a was Created in BioRender. Cohen, M. (2023) https://BioRender.com/q62w962.

(Fig. 3C, D). Lentil and chickpea proteins showed better mechanical properties, about 88% to 97% higher than oleogel ($p < 0.001$). Pea protein showed G′ and G″ that were 129% and 118% higher than oleogel, respectively ($p < 0.001$). Soybean was 160% and 83% higher than oleogel, respectively ($p < 0.001$). Mung bean protein stood out with G′ and G″ that were 214% and 168% higher than oleogel, respectively ($p < 0.001$). The data demonstrated distinct rheological properties of soybean and mung bean-stabilized oleogels that were further evaluated in high temperatures.

Biomechanical characterization of proteoleogel metamaterial (PToG)

To study the thermal stability of proteoleogel (PToG) we heat-treated beef fat, oleogel, and mung bean proteoleogel at 85 °C for 10 min in a water bath. Visual inspection showed that while the viscosity of oleogels increased, proteoleogels appeared to solidify at a higher temperature (Supplemental Movie S1). Scanning electron microscopy showed the structured matrix of denatured beef fat, with distinct anchoring features (Fig. 4A). Interestingly, while oleogels showed a smooth appearance, proteoleogels showed complex overlapping spherical contusions emulating the ultrastructural appearance of animal fat (Fig. 4A).

To compare the mechanical behavior of the new material to animal fat, we compared oleogels and proteoleogels to beef fat (Fig. 4B–E). Force–displacement plots show mechanical resilience, a critical determinant of material integrity (Fig. 4B). The elastic strain energy, a quintessential indicator of textural robustness, revealed that oleogels retained approximately 52% of beef fat's characteristic energy, whereas proteoleogels are not significantly different from beef fat at 97% (Fig. 4C). The maximal load of proteoleogels was similarly indistinguishable from animal fat, underscoring this metamaterial potential to replicate the tactile appeal of beef fat.

Stress-strain curves showed similar dynamics, with proteoleogels showing a deformation recovery profile like beef fat (Fig. 4D). Further analysis showed similar results for the proteoleogels' toughness and tensile strength. When contrasted against beef's benchmarks, oleogels manifested 50% and 23% efficacy for toughness and tensile strength, respectively ($p < 0.001$). In contrast, PToG closely mirrored beef fat's biomechanical attributes, registering at 95% and 105%, thereby alluding to their advanced architectural congruence with traditional beef fat (Fig. 4E).

To evaluate proteoleogels during cooking, we carried out visual and tactile experiments on a hot surface at 150 °C to 250 °C. Grilled proteoleogel solidified similarly to beef fat, whereas the standard oleogel behaved like egg-white (Fig. 4F, Supplementary Movie S1). To demonstrate the ability of proteoleogel to bind protein, we developed and grilled a 1.5 cm thick-cut wagyu-like steak, bound together by the proteoleogel metamaterial (Fig. 4G). The thick-cut steak maintained its structure throughout the grilling process, undergoing Maillard browning at 165 °C. Cutting the steak demonstrated strong binding of proteoleogel to LTMA (Fig. 4G).

Blinded sensory test of injection molded products

To test the ability of our process to replicate the taste and texture of whole cuts, we produced injection-molded lamb chops using proteoleogel and LTMA. Both injection molded product and farmed meat were cooked by grilling on a hot skillet at about 200 °C for 5 min showing similar browning (Fig. 5A, B). The nutritional profile of farmed and injection molded products was comparable (Fig. 5C).

Next, we performed a blinded sensory tasting analysis, involving 23 participants with varying demographic and dietary characteristics (Fig. 5D). 65% of the study group identified as meat eaters, 17% identified as flexitarian, and 9% as vegetarian (Fig. 5D). Study participants received brief training, and sequentially rated fully-cooked farmed meat, HMMA-based control, and LTMA-based products. The product sequence was randomized. Flavor and physical attributes were ranked from 0 (noting "insufficient") to 20 (marking "excessive") attribute. Study participants easily identified farmed meat which scored 10, (noting "just right") on all attributes (Fig. 5E). The HMMA scored 7 on average, while LTMA-based product scored 10 on average, similar to beef, participants noted a strong aftertaste and insufficient meaty flavor. Participants also assessed texture-related physical attributes, including dryness/juiciness, texture, color intensity, appearance, and aroma (Fig. 5F). The physical attributes of HMMA scored 5 on average, compared to 10 for farmed meat. Study participants rated LTMA as 9 on average noting marginally softer texture and more intense color than farmed beef. Forced choice test revealed that 57% of participants preferred beef, 43% preferred the LTMA, and none preferred HMMA (Fig. 5G).

Thermal profiles of LTMA meat analogs

Exploded CAD views show the injection molding process for precision cuts of wagyu steak, lamb chop, and T-bone cut (Fig. 6A). This approach not only allows for the manipulation of shape but also permits the engineering of distinct thermal behaviors and properties within each cut. Upon grilling at 200 °C for 5 min, LTMA cuts exhibit uniform browning, with the wagyu steak revealing its marbling and the lamb chop and T-bone maintaining an authentic balance of meat, fat, and bone (Fig. 6B). In the thermal analysis, conducted via a finite-element model in SolidWorks, we infused the cuts with varying thermal properties assigning thermal conductivities of 0.52 and 0.23 W/(m·K) for meat and fat, respectively. This revealed an intense heat flux surrounding the fat marbles of the wagyu steak, while the lamb chop demonstrated elevated heat flux in fattier regions. The T-bone steak, however, exhibited a more even heat distribution, a testament to its leaner makeup (Fig. 6C).

Temperature gradient analysis offered further insight, highlighting the wagyu steak's intricate thermal behavior, pinpointing localized high-temperature areas in the lamb chop, and marking a notable temperature gradient near the bone of the T-bone steak (Fig. 6D). These discernments unravel the nuanced ways in which fat distribution and cut design influence cooking responses and, consequently, the doneness profiles of different meat cuts.

Crucially, the variability in the thickness of the cuts, 10 mm for both lamb chop and wagyu, and 16 mm for T-bone, along with the strategic distribution of metamaterials, underscored the capability of injection molding to revolutionize the entire product's behavior, transcending mere shape alteration. This comprehensive analysis thereby offers invaluable guidance to culinary professionals and food scientists, illuminating pathways toward optimizing texture and sensory appeal in cooked meats.

Techno-Economic Analysis (TEA) of injection molding

Detailed technical economic analysis (TEA) of injection molding versus 3D printing is shown in Supplementary Tables S1–10. Analysis was broken down into capital investment, operating costs, and production costs (Fig. 7A–C). The size of the production floor was kept constant at 200 m^2. The analysis projected one low-temperature extruder working at 90 kg/h, compared to four 3D printers working at 24 kg/h. Total direct cost (TDC) in injection molding was 23% lower than 3D printing due to equipment cost. This results in an 18% difference in total capital investment (TCI) (Fig. 7A, D). Analysis of raw materials showed little difference in cost per kg. However, the low output of the 3D printing facility drove the cost of utilities to $4.4 per kg compared to $1.3 per kg for an equivalent injection molding facility due to the difference in output.

The main difference between injection molding and 3D printing came down to labor (Supplementary Tables S1–10). The 3D printing facility required automation engineers, and 34 batch workers in our analysis compared to 15 working in an equivalent injection molding

https://doi.org/10.1038/s41467-024-54939-y

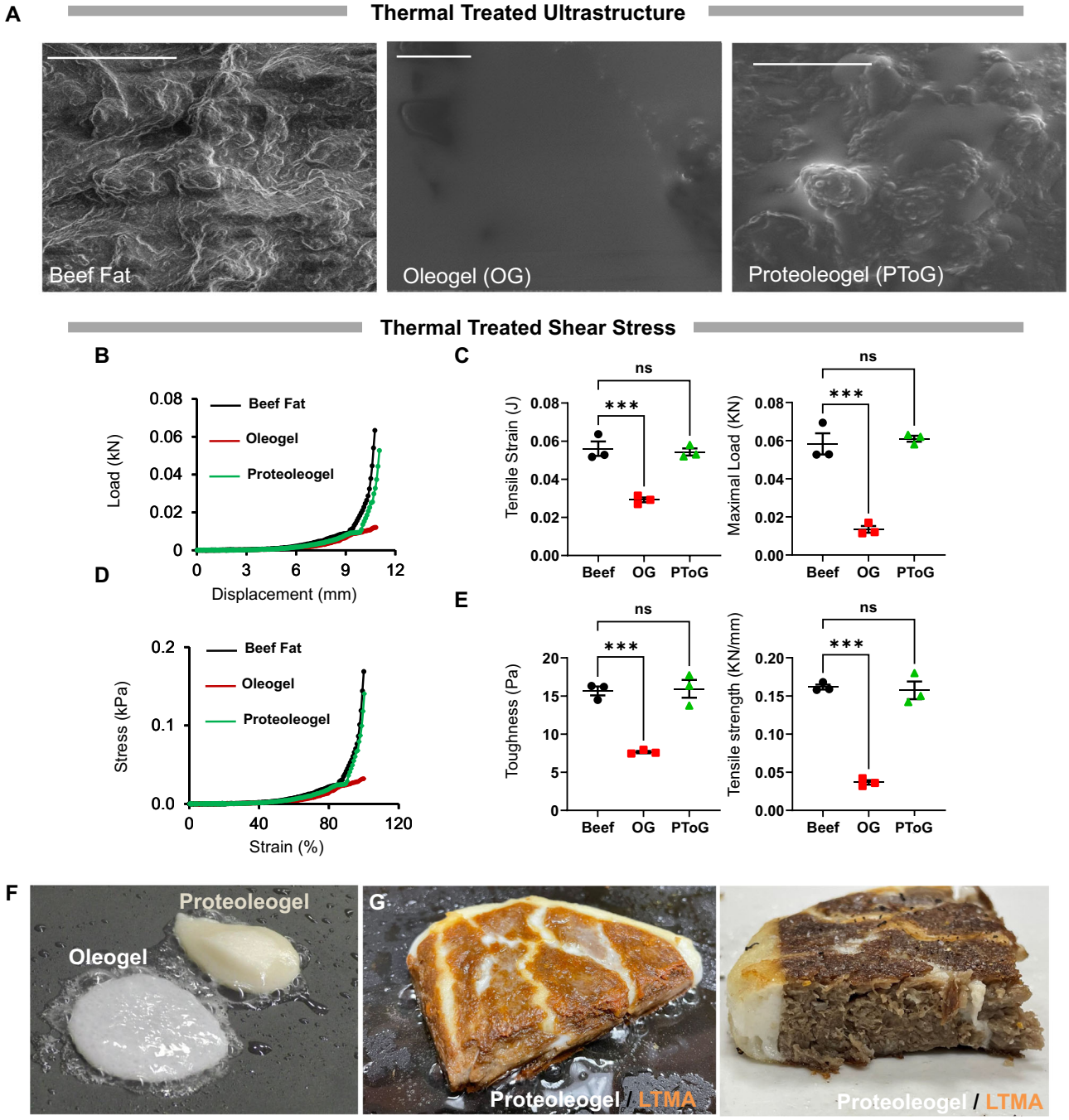

Fig. 4 | Structural and mechanical profiling PToG metamaterial post-cooking. **A** Scanning electron micrograph of cooked beef fat (*left*) shows a complex microscale matrix with distinct anchoring features. Standard cooked oleogel shows a homogenous smooth structure (*middle*). Mung bean protein-based PToG (*right*) shows complex microscale organization with anchoring features reminiscent of animal fat. Scale bar = 100 μm. **B** Force–displacement curves of cooked beef fat, standard oleogel, and PToG demarcate the mechanical resilience of each material. **C** Analysis of elastic strain energy shows that oleogels hold 52% of beef fat's elastic energy ($p < 0.001$, $n = 3$), PToG was not significantly different from cooked beef fat. (ns $P > 0.05$, ***$P \leq 0.001$; $n = 3$). Significance was determined using a one-way ANOVA with Dunnett correction. **D** Stress-strain curves of cooked beef fat, standard oleogel, and PToG show similar biomechanical behavior of PToG metamaterial compared to beef fat. **E** Both toughness modulus and ultimate tensile strength showed oleogels achieve 50% and 23% efficacy of beef fat for toughness and tensile strength respectively ($p < 0.001$, $n = 3$). In contrast, PToG's biomechanical attributes after cooking were not significantly different from traditional beef fat, confirming the complexity of their structure. (ns $P > 0.05$, *** $P \leq 0.001$; $n = 3$). Significance was determined using a one-way ANOVA with Dunnett correction. **F** Visual assessments of cooked PToG compared to oleogel show shape memory-retentive behavior mirroring beef fat, while standard oleogel flows like raw egg white. **G** To demonstrate integration of PToG and LTMA metamaterials we formed a wagyu-like steak. Cooked PToG bound LTMA in a similar manner to connective tissue (e.g., fat). Materials could be cut showing strong bonds between the materials in intersections. All n values represent the number of experimental repeats. Error bars indicate ± s.e.m.

https://doi.org/10.1038/s41467-024-54939-y

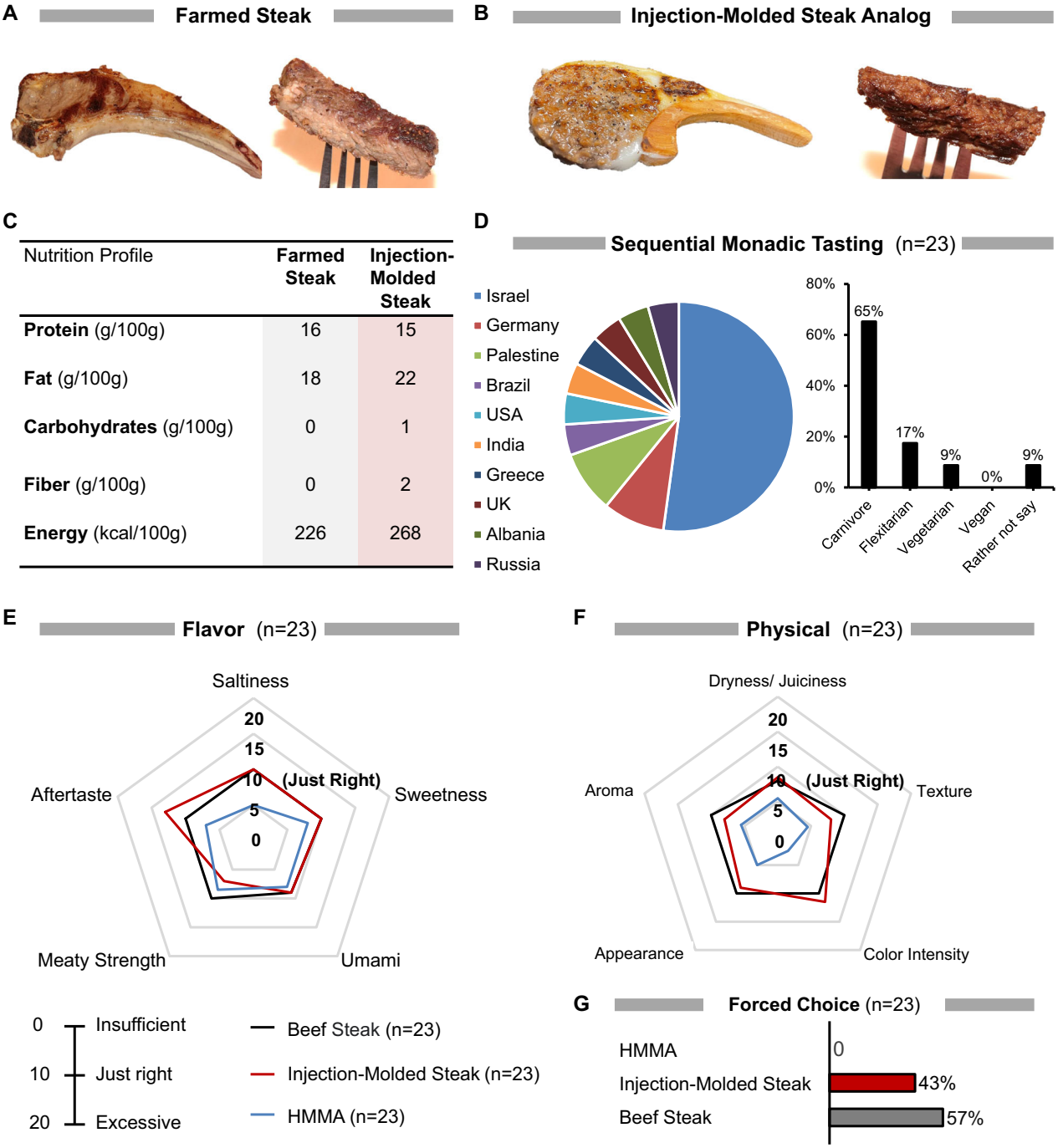

Fig. 5 | Blinded tasting of farmed meat cuts, injection molding-based product composed of LTMA and PToG metamaterials and the HMMA base. A Photo of farmed lamb chop (*left*) and beef steak tip (*right*). **B** Photo of injection-molded lamb chop analog composed of LTMA and PToG (*left*) and steak tip analog composed of LTMA (*right*). Products are similarly cooked and lightly seasoned. **C** Nutritional analysis comparing farmed steak with injection molded steak analog composed of LTMA and PToG. **D** Demographic and dietary characteristics of participants ($n = 23$) in a sequential monadic blindedtasting experiment. Meat eaters constituted 65% of the group. For simplicity, the blinded test was divided into flavor-related (**E**) and texture-related (**F**) attributes. **E** Products were scored from 0 to 20 on saltiness, sweetness, umami, meaty strength, and aftertaste. LTMA's ratings on these attributes were closer to beef, whereas HMMA had a noticeable difference, particularly in meaty strength and aftertaste. **F** Participants also rated the samples on texture and sensory attributes, including dryness/juiciness, texture, color intensity, appearance, and smell. The injection-molded LTMA product received ratings closer to beef in all aspects except color intensity. HMMA was rated lower than beef across all attributes. **G** The sensory analysis was followed by a blinded forced-choice study. 57% of participants preferred farmed steak, 43% the injection -molded LTMA product, and none preferred HMMA ($n = 23$).

facility. Our analysis revealed a cost of goods sold (COGS) of $8.9 per kg for injection molding steak, compared to $38.4 per kg for a 3D printing facility (Fig. 7C, F). Our technical economic analysis suggests that even a small-scale production facility for whole cuts could be economical, producing whole cuts below the market costs of steaks and chops. Expanding upon the initial economic evaluations, a comparative assessment of labor and utilities costs per kilogram between the two facilities was conducted (Fig. 7E). The findings highlighted a substantial difference in the workforce requirements, with the 3D printing facility necessitating a

https://doi.org/10.1038/s41467-024-54939-y

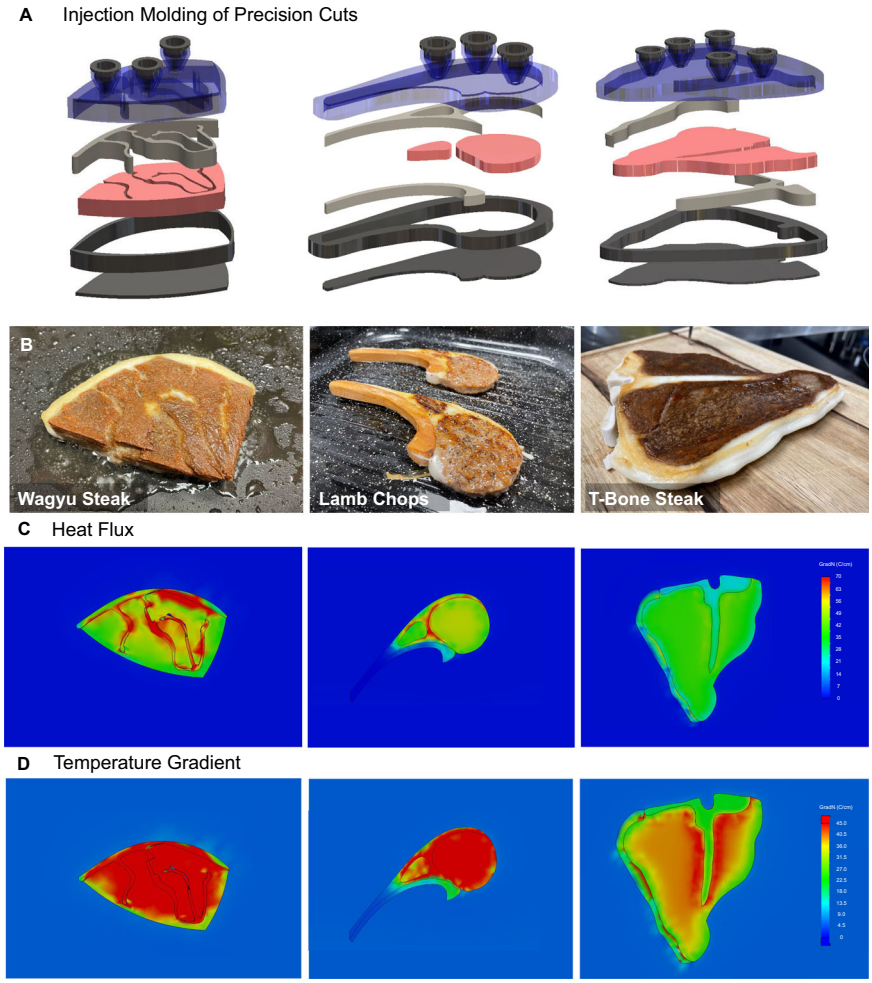

Fig. 6 | Design and varied application of injection -molded whole cuts. **A** Exploded CAD views of the injection molding process for high-fat wagyu steak (*left*), thin lamb chop (*middle*), and a thick, bone-heavy T-bone steak (*right*). **B** Photos of cooked injection-molded wagyu steak (*left*), lamb chop (*middle*), and T-bone steak (*right*). Each cut was grilled at 200 °C for 5 min, demonstrating similar browning characterizing the Maillard reaction. **C** Heat flux is shown in °C/cm. Wagyu steak analog showed low thermal resistance due to the abundance of PToG fat marbling resulting in high heat fluxes (*red*) along the interfaces and faster cooking. In contrast, the T-bone steak showed more homogenous heat distribution due to its leaner composition and the thermal resistance of the central bone (*cyan*). As expected, lamb chop showed a mixed behavior. **D** Analysis of temperature gradient map across wagyu steak (*left*), lamb chop (*middle*), and T-bone steak (*right*). The surface of the marbled wagyu steak was rapidly heated due to its PToG-rich structure. Lamb chop showed a similar heat pattern in the LTMA due to its thickness. Finally, the T-bone steak exhibited a notable temperature gradient near the bone-meat interface, a region often enriched with fat, which may result in a more consistent but less nuanced flavor profile. These variations in cooking temperatures underscore the ability of injection molding to create varied and distinct products for multiple meat applications.

significantly larger team of automation engineers and batch workers compared to the leaner workforce at the injection molding facility, contributed notably to the COGS, with labor costs amounting to $2.8 per kg for injection molding and $24.63 per kg for 3D printing, revealing an 89% cost reduction in injection molding. On the utilities front, injection molding proved to be more economical, incurring costs of $1.31 per kg, over three times lower than the $4.38 per kg seen in 3D printing.

Discussion

The quest for sustainable meat alternatives reached a pivotal juncture. While plant-based ground meat analogs have made significant inroads[43], the cost-effective production of whole cuts which make up 54% of the global market remained an elusive goal. Our study introduces a paradigm shift by employing injection molding, a technology hitherto confined to the polymer industry[44], to produce whole cuts of meat analogs. This approach not only addresses the multiscale complexity inherent to meat but also offers an economically viable pathway for mass production.

Metamaterials display properties that come from their carefully designed structure rather than their composition. Recently, Souto and colleagues used 3D printing to create anisotropic fracturing in chocolates and other confectionaries[45]. Here we describe two metamaterials, low-temperature meat analog (LTMA) and proteoleogels (PToG) that mimic the micro- and mesoscale structures of muscle and fat, respectively. LTMA utilizes textured vegetable protein which already has a fibrous structure formed by high-temperature extrusion. The fibers are then embedded in a gel and compressed in a cooling step that creates a multiscaled metamaterial. Ultrastructure analysis showed fibers that are 200 ± 50 μm in diameter, not different from muscle, closely packed into fascicle-like structures 1.2 ± 0.3 mm in diameter, which are organized into bundles about 5 mm thick (Fig. 2E, F). Complex organization plays a key role in the mechanical properties of beef muscle[29] and LTMA.

As HMMA could not be injected, our mechanical analysis focused on extruded products with similar protein and fat composition (Fig. 2). While in the longitudinal section, the textural characteristics of beef and LTMA were similar, differences existed in maximal load and

https://doi.org/10.1038/s41467-024-54939-y

A

Capital Investment	Injection Molding	3D Printing
Equipment Capacity	100 kg/h	24 kg/h
ISBL Direct Cost	$1.7 M	$2.4 M
OSBL Direct Cost	$0.2 M	$0.2 M
Building Cost	$1.2 M	$1.2 M
Total Direct Cost (TDC)	$3.1 M	$3.8 M
Engineering & Construction	$1.1 M	$1.3 M
Fees & Contingency	$0.6 M	$0.8 M
Total Capital Investment (TCI)	$4.9 M	$5.8 M

B

Operation Costs	Injection Molding	3D Printing
Total Ingredients ($/kg)	$2.7	$2.9
Total Utilities ($/kg)	$1.3	$4.4
Variable Operating Costs ($/kg)	$4.0	$7.2

C

Production (COGS)	Injection Molding	3D Printing
Total Labor Costs ($/kg)	2.8	24.6
Total Fixed OPEX ($/kg)	4.7	30.9
Total Cost of Production ($/kg)	**$8.9**	**$38.4**

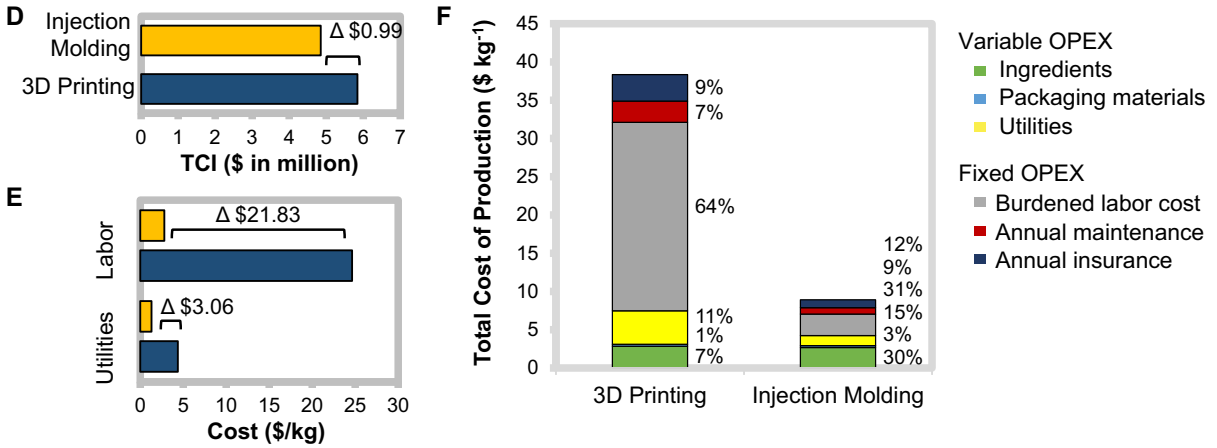

Fig. 7 | Techno-Economic Analysis (TEA) of injection molding vs. 3D printing. **A** TEA comparing injection molding and 3D printing technologies, focusing on Capital Investment, Total Direct Cost (TDC), and Total Capital Investment (TCI) detailed in Supplementary Tables S1–10. An injection molding extrusion line has a capacity of 100 kg/h. **B** Difference in operational costs was primarily driven by the 4-fold difference in capacity. Variable operating costs were $4 per kg for injection molding, 44% less than $7.2 per kg for 3D printing. **C** Comparison of labor costs and the cost of goods sold (COGS). **D** Analysis of the total capital investment (TCI), which considers construction expenses for the production facilities in both methodologies, encompassing various aspects such as area, levels, and building component costs, reveals an 18% disparity. This calculation incorporates indirect costs, engineering expenditures, and construction-related expenses detailed in Supplementary Tables S1–10. **E** Comparative analysis of labor and utility costs per kilogram between injection molding and 3D printing facilities. Injection molding requires significantly fewer workers, contributing to much lower labor costs. Utility costs were also lower for injection molding than for 3D printing. **F** Graph depicting a comparison of variable and fixed operating expenses (OPEX) between 3D printing and injection molding technologies. Injection molding shows lower variable OPEX compared to 3D printing. Fixed OPEX is also lower for injection molding. Maintenance and insurance costs follow the same trend.

ultimate tensile strength in the perpendicular section. This assessment demonstrates the similar chewiness and resilience of LTMA and beef, contrasting with the softer gummy behavior of HMMA. Biting LTMA in the perpendicular direction would offer more resistance than HMMA but is still about 15% softer than beef (Fig. 2K–N). While the softer texture of LTMA was noticeable by the participants of the sensory analysis (Fig. 5F) it did not seem to distract from the product appeal in the forced choice (Fig. 5G).

Blinded taste tests further corroborate the sensory fidelity of the injection-molded meat analogs, with a 43% preference rate. We note that whole cuts are seldom consumed *well done* giving somewhat of an advantage to LTMA over beef cuts and may not represent typical consumer preference. While this may not yet match the acceptance level of traditional meat, it signifies a substantial advancement in the field, especially considering the complexity of whole cuts. However, our sensory evaluation was limited by a small sample size and a lack of demographic diversity. Future research should involve larger, more diverse populations to validate these findings. Additionally, the aftertaste of LTMA, which was higher than desired (Fig. 5E), suggests the need for further flavor and aroma optimization before the full potential of the technology could be realized.

The economic analysis further underscores the advantages of injection molding. Initial setup costs for injection molding are high, but they decrease with production scale as these costs are spread over more units. Conversely, 3D printing has lower initial costs but higher variable costs that remain constant, limiting cost reduction at larger scales. Labor and utility costs highlight a substantial difference in workforce requirements, with 3D printing facilities needing a significantly larger team of automation and mechanical engineers and batch workers. In contrast, injection molding facilities, which are semi- or fully- automated, require a leaner workforce. This difference in labor costs significantly reduces the cost of goods sold (COGS) for injection molding.

Additionally, the long-term environmental impact of sourcing plant proteins at scale remains to be assessed. Future work should also explore the nutritional optimization of these meat analogs, particularly in terms of bioavailable nutrients and amino acid profiles.

In conclusion, our work heralds a new era in sustainable food technology by offering a scalable and economically viable method for producing whole-cut meat analogs. The injectable metamaterials developed herein hold the potential to revolutionize the meat substitute market, thereby contributing to a more sustainable and ethical food ecosystem.

Methods

Meat and meat analogs

Beef fat and meat tissue were resected from a commercially available 8-month-old Holstein beef ribeye steak, and lamb chop was obtained from a commercially available 6-month-old Awassi sheep. High-moisture meat analogs (HMMA) were purchased as Garden Gourmet® Vegan Fillet Pieces (Nestle, Switzerland).

Meta-analysis of economic distinctions between injection molding and 3D printing

Quantitative data elucidating the economic distinctions between injection molding and 3D printing were collected from literature reviews that intricately compare 3D printing and injection molding technologies in plastic part production[46–48]. The datasets were standardized for production volumes to allow comparative analysis, analyzing machine, tooling, and labor expenditures.

Advanced injection molding process design and modeling

Computer-aided design (CAD) models detailing the sequential stages of the advanced injection molding process for the replication of complete meat analogs were done using Solidworks 2017 (Dassault Systèmes, France). This software was used to detail the intricate structures, transitions, and nuances intrinsic to the meat analog replication process.

The production and products produced were documented using a Canon EOS 750D camera and were used to validate the design and processes constructed. Each distinct phase of the advanced injection molding procedure was captured in real-time, focusing on the transformation of raw materials to the final meat analog of entrecote steak. Each photograph corresponds to a particular stage in the CAD model, ensuring the comprehensive representation of the process, both virtually and physically.

Proteoleogel preparation

Oleogels were formed using high-shear emulsification of a mixture of 2.5% w/v methylcellulose (VIVAPUR, Germany), 30% canola oil (Poliva, Israel), and 67.5% water using a KMC3000 mixer (Sauter, Switzerland) with controlled stirring settings. Briefly, methylcellulose and canola oil were mixed at 135 rpm for 3 min. Subsequently, water was gradually added, and the stirring speed was increased to 180 rpm for an additional 5 min. To ensure uniformity, both the materials and ambient conditions were maintained at 20 °C.

Proteoleogels were formed using high-shear emulsification of a mixture of 2.5 w/v protein isolate or concentrate, 2.5% w/v methylcellulose (VIVAPUR, Germany), 30% canola oil (Poliva, Israel), and 65% water using a KMC3000 mixer (Sauter, Switzerland) with controlled stirring settings. Briefly, 2.5% w/v of CP-PRO70 chickpea protein (70%, InnovoPro, Israel) or Solanic300 potato protein (80%, Avebe, Netherlands) or ProFam974 soybean protein (90%, ADM, USA) or pea protein isolate (80–90%, Hama Industrial Chem, Israel) or mung bean protein isolate (70–80%, Hama Industrial Chem, Israel) or lentil protein concentrate (50–75%, Hama Industrial Chem, Israel) or rice protein isolate (80–90%, Hama Industrial Chem, Israel). Methylcellulose, and canola oil were mixed at 135 rpm for 3 min. Subsequently, water was gradually added, and the stirring speed was increased to 180 rpm for an additional 5 min. To ensure uniformity, both the materials and ambient conditions were maintained at 20 °C. The high shear emulsification facilitated the uniform integration of the protein isolates and methylcellulose in the oil, ensuring fine dispersion of particles and resulting in a stable, homogeneous mixture. A hydrogel form is formed exhibiting structural integrity reminiscent of animal fats.

Rheological characterization

The rheological analysis of hydrogels was carried out using Modular Advanced Rheometer System MARS™ (HAAKE™ III, Thermo Scientific) as previously described[49]. Briefly, 350 μL samples of oleogels and proteoleogels were placed on the rheometer's base. Initial evaluations involved frequency sweep tests at different 14 frequencies, ranging from 0.1 to 14 Hz, which were conducted to identify optimal conditions (Supplementary Fig. S2A) Based on the frequency sweep test, 1 Hz sweep rate tests were performed on all samples. Tests were conducted at a controlled temperature of 20 °C and a 1% strain. Every batch was tested in three replicates (technical repeats) and a total of five batches per sample were measured (replicates) to ensure the accuracy and repeatability of the results.

Gelation dynamics test was carried out using Modular Advanced Rheometer System MARS™ (HAAKE™ III, Thermo Scientific) as previously described[50]. Briefly, rheological measurements of storage modulus and loss modulus were performed during a temperature ramp, gradually increasing the temperature at a controlled rate of 1 °C per second to 85 °C. (Supplementary Fig. S2B). The gelation temperature was determined at the point where the storage modulus exceeds the loss modulus, indicating the transition from a liquid-like to a solid-like state as the gel solidifies.

Low-temperature extruder design and fabrication

The design of a low-temperature extruder was done in SolidWorks 2017 (Supplementary Fig. S3A). Based on the CAD, each component was fabricated at a 30 μm resolution using a 5-axis CNC machinery at the Racah Institute of Physics, Faculty of Mathematics and Natural Sciences, The Hebrew University.

A single-phase AC 220 V, 300 W, 1350 rpm motor (HST M6300, China) with a gearbox motor boasting a ratio of 1:54 (HST 5GN, China), and the speed control unit (US-52 ManHwa, China) was integrated into the fabricated assembly. This mechanical synergy enabled rotational speeds between 0-25 rpm to modulate the motor speed with precision. A consistent operating temperature of 85 °C in the barrel was maintained using a 400 W stainless steel heater band mica heating elements (CNTOPHEAT, China), precisely regulated by a digital PID controller (REX-C100 LEFAVOR, China) to 85 °C ± 2 °C.

The extruder's single screw was a focal element, designed with a length of 410 mm, featured a pitch distance of 30 mm, a pitch height of 3.5 mm, and a pitch thickness of 5 mm, constructed from hard chrome-plated steel to ensure optimal performance and heating conductivity.

CAD designs of molds for precision cuts

CAD design of entrecote, waygu, lamb chop, and T-bone molds were created using the *Sketch From Photo* feature in Solidworks 2017 to design analogs with a high resemblance to meat counterparts in appearance. Briefly, high-definition images of different meat cuts were taken using a Canon EOS 750D, focusing on the intricate details and unique textures that characterize each cut. The images were then imported into SolidWorks 2017, where the *Sketch Picture* feature was employed. Each image was scaled and oriented accurately to match the actual dimensions and structure of the respective meat cuts. Various sketch tools were employed to capture every nuance of the meat and the fat outlines, distinctive features were traced and captured, ensuring an authentic reproduction. The sketches were then transformed into 3D models with defined depth and volume using the extruded base feature of Solidworks 2017. Further refinements to create the molds of the meat cuts were done using *Fitting*, *Extruded Cuts*, *Lofted*, and *Swift Boss* Features.

The CAD designs were fabricated from RGD525, biocompatible digital ABS Plus, VeroBlackPlus, VeroWhitePlus, and SUP706, at a resolution of 30 μm using a Connex3 Objet260 3D printer (Stratasys, Israel). The 3D-printed parts were cleaned from the support material (SUP706) overnight in 2% sodium hydroxide and 4% sodium metasilicate solution. The printed parts are composed of the mold core, mold cavity, main runner, and bottom clamp plate. Before use, the complete

system was cleaned overnight in 70% ethanol and sterilized for 3 h in UV light as previously described[51].

Bone analog preparation

Bone analogs were fabricated by molding synthetic bone cement into bone-shaped molds. Briefly, CAD designs of T-bone, entrecote, and lamb chop bones were created using the *Sketch From Photo* feature in Solidworks 2017 to design analogs with a high resemblance to bone counterparts in appearance. Briefly, high-definition images were taken using a Canon EOS 750D, focusing on the intricate details and structures that characterize each bone type. The images were then imported into SolidWorks, where the *Sketch Picture* feature was employed. Each image was scaled and oriented accurately to match the actual dimensions and structure of the respective bone. The sketches were then transformed into 3D models.

Synthetic bone cement was created through rigorous mixing using a KMC3000 mixer of 10% w/v of beta-tricalcium phosphate powder (21218 Sigma-Aldrich, USA), 50% w/v of calcium sulfate powder (23713 Sigma-Aldrich, USA), and 40% w/v solution of polyvinyl alcohol (341584 Sigma-Aldrich, USA) at 135 rpm for 5 min. The procedure is conducted at ambient room temperature.

Immediately after mixing, the cement paste is carefully poured into the molds, shaping the material for different bone shapes, and allowed to harden for 8 min uninterrupted, ensuring that the cement reaches its optimal, solidified state. The solidified bone analogs were extracted from the mold and baked in a 65 °C oven for 1 h.

Preparation of raw materials for LTMA production

The synthesis of the raw material destined for LTMA production involved the hydration of 16% w/v textured vegetable protein (TVP) using 48% w/v water over a period of 1 h. Both the materials and ambient conditions were maintained at 20 °C. The hydrated mixture was then subjected to a rigorous stirring process using a KMC3000 mixer, operating at a steady pace of 135 rpm for 20 min. 27% w/v mung bean-based proteoleogel, created as previously described, was gradually added to the mixture through continued stirring at 135 rpm for 5 min. Once the mixture had settled, 4% w/v soy isolates, 4% w/v potato protein, and 1% w/v beef flavor (TQ3056883 Givaudan, Switzerland) were added. The final mixture was then subjected to a rigorous stirring process by a KMC3000 mixer, operating at a steady pace of 180 rpm for 15 min.

LTMA extrusion processing

LTMA products were created using a low-temperature single-screw extruder (Supplementary Fig. S3B; Supplementary Movie S2). While the standard production of HMMA is extruded at high temperatures (Supplementary Fig. S3C). Briefly, LTMA mixture was added to the feeder, and processed within the barrel at a stable, uniform 85 °C at a screw speed of 14 rpm (Supplementary Fig. S3D). The introduction of the mix into the extruder was done at a consistent outflow rate of 10 ± 2.5 kg/h. After processing, the LTMA was extruded through a 50 × 20 × 70 mm ($W \times H \times L$) die into molds or sectioned, collected into plastic bags, and vacuum sealed.

Injection molding process

The formation of our meat analogs was characterized by a sequential process of each component—bone, muscle, and fat—to replicate the complexity of real meat cuts like steaks and chops (Supplementary Fig. S1B, C). Briefly, suitable bone analogs were positioned within the designated steak molds. LTMA mixture was extruded into two bone-containing molds at 10 ± 2.5 kg/h for 3 min. Computational fluid dynamics, using SolidWorks 2017, was carried out to test the flow trajectory of the extrudates and the pressure inside the mold, (Supplementary Fig. S2C; Supplementary Movie S3). At this point, the bone and protein were extracted, and a fat mold was placed. Proteoleogel was injected into the fat mold 12 ± 1 kg/h for 30 s. The proteoleogel flowed into the spaces left by the top mold removal, effortlessly filling the voids amidst the molded muscles where it gelled and created a seamless integration between the muscles, fat, and bone structures. The cut was then removed from the mold and placed onto a Peltier cooling unit (XD2029 Tonfishi, China) set at 4 °C for 5 min. The cut was then placed into a plastic bag, vacuum sealed, and stored at −18 °C. Prior to freezing, samples of the cuts underwent microbiological testing, confirming the negative for Salmonella Class II and *E. coli*, with yeast and mold at a maximum of 100 cfu/g, and coliforms at a maximum of 10 cfu/g.

Force-displacement analysis

Mechanical analysis focused on extruded HMMA and LTMA samples, as HMMA could not be injected. Samples of beef meat, extruded high-moisture meat analogs (HMMA), and extruded low-temperature meat analogs (LTMA) were cooked using a Sous vide method as previously described[52]. 30 g samples of Beef, HMMA, and LTMA were vacuum sealed in a plastic bag and then submerged in a water bath at a steady temperature of 55 °C for 3 h. Cooked samples were precisely cut into 22 mm × 22 mm × 15 mm sections. The cuts were subjected to force-displacement tests using an 1114 Instron testing machine (Instron, USA).

2 g samples of beef fat, oleogel, and proteoleogel samples were placed in a 15 mL plastic conical tube and submerged in a water bath at a steady temperature of 85 °C for 10 min. Cooked samples were cut into 10 mm × 10 mm × 15 mm sections. The cuts were subjected to force–displacement tests using an 1114 Instron testing machine (Instron, USA).

The tests were performed in a controlled environment at 21 °C and 40% relative humidity, with machine settings fine-tuned to a data rate of 10 pts/s and crosshead speed of 10 mm/min. Each test was conducted on three samples from each batch (technical triplicates) in three different batches (replicates) to ensure precision and reproducibility. Mechanical properties of the samples were gauged based on the orientation of fibers, evaluating elastic strength for perpendicular fiber orientation and tensile strength for longitudinal orientation.

Force-displacement data was analyzed utilizing an *Area Under the Curve* method in GraphPad Prism 9 (GraphPad, USA). The tensile strain energy was determined by the area under the stress-strain curve. The toughness modulus was computed as the rate of energy absorption normalized by sample volume. The maximal load was determined by the peak force recorded, while the ultimate tensile strength was determined by the peak stress recorded before the sample was destroyed.

Thermal simulations of LTMA precision cuts

Thermal simulations of wagyu steak, lamb chop, and T-bone steak were done using the steady-state thermal study in Solidworks 2017 at an ambient temperature of 20.85 °C and 1 atm of pressure. Using the meat cuts CAD designs created as previously described, they were placed on top of a CAD-designed iron skillet. The simulation was done using the specific essential thermal properties[53–56]. For the meat parts, a thermal conductivity of 0.52 W/(m·K), mass density of 1100 kg/m^3, and specific heat of 3600 J/(kg·K) were set. For the fat part, thermal conductivity of 0.23 W/(m·K), mass density of 900 kg/m^3, and specific heat of 2200 J/(kg·K). For the bone part and iron skillet, default ceramics and iron parameters were used from the SOLIDWORKS material database, respectively.

The skillet was adjusted at 3500 W power, heating source was applied to the bottom of the skillet and the temperature was set at 230 °C. The wagyu steak, lamb chop, and T-bone steak surfaces were placed directly on the designed skillet surface. Heat flux distribution across the entire surface of the meat cuts and temperature gradients

across the thickness of the steaks were analyzed and presented as heat maps, coded to display the highest values in red and the lowest in green.

Scanning electron microscopy (SEM) and stereo microscopy

Farmed beef, HMMA, and LTMA were cooked in a Sous vide method for meat as previously described[52]. Briefly, samples with a thickness of 2 cm were vacuum sealed in a plastic bag and then submerged in a water bath at a steady temperature of 55 °C for 3 h. Beef fat, oleogel, and proteoleogel samples were cooked in sous vide method for fat as previously described[57]. Briefly, the samples were vacuum sealed in a plastic bag and then submerged in a water bath at a steady temperature of 85 °C for 10 min.

After cooking, all samples were carefully cut into 1 mm thick sections using a slicer for Stereo Microscopy imaging and into holder-suitable 4 × 4 × 2 mm sections for SEM analysis. The 1 mm thick sections were imaged using a Stereo Microscope (ZEISS Stemi 508) to investigate the gross fascicle structure in beef, HMMA, and LTMA. Multiple optical images were quantified to resolve gross fascicle width.

After cooking, all samples were carefully cut into holder-suitable 4 × 4 × 2 mm sections and mounted on SEM holders. The cooked samples were then precoated with an Au–Pd nanolayer using an SC7640 Sputter Coater (Polaron, England). Scanning Electron Microscopy (SEM) imaging was conducted using an FEI Sirion High-Resolution Scanning Electron Microscope (HR SEM, Holland) at the Center for Nanoscience and Nanotechnology, The Hebrew University, employing optimized parameters for detailed image capture. These included secondary electron (SE) detection, an accelerating voltage of 5 kV, a spot size of 4.0, and a working distance of 5.3 mm in high-resolution mode. An additional TSL-EDAX (EDAX, USA) system was mounted for electron back-scattered diffraction analyses to provide intricate details of each sample's structural composition.

The quantification of fiber diameter in SEM images was performed using ImageJ software. SEM images were uploaded into ImageJ Fiji Software, and the scale was calibrated based on the provided scale bar. Regions of interest (ROI) were manually selected where fibers were clearly visible. Using the line tool, measurements were taken across the diameter of fibers within the selected ROI. The average fiber diameter was calculated from these measurements.

Sensory evaluation of products

Products, including injection-molded steak analog formulated from proteoleogel and LTMA, were prepared as previously described. Injection-molded lamb chops, HMMA-based meat analog, and farmed meat underwent a uniform cooking process, seared at 200 °C for 5 min on a hot skillet and seasoned using 1-g salt and 1-g black pepper.

A blinded product tasting was carried out following the approval of the Hebrew University of Jerusalem Institutional Review Board. In this sequential monadic test, 23 diverse, untrained, participants tasted the injection-molded meat analog, farmed meat, and the textured protein base (HMMA), one at a time. The tests were performed in groups of 5–6 people. They were asked to assess the sensory attributes of the cooked products. During the tasting session, participants were asked to rate the products according to various texture-and flavor-related attributes, including intensity of saltiness and sweetness, umami and meaty flavors, aftertaste, dryness or juiciness, color intensity, appearance, and aroma. Each attribute was scored on a scale of 0 to 20 (0–too mild/dislike, 10–just right, 20–too strong/like). Rating was carried out with a pencil and paper questionnaire (Supplementary Table S11). Participants were then prompted to make a forced choice, selecting their preferred product from the options presented. The participants were invited to elaborate and explain their choice or comment on anything else. Finally, the participants were invited to indicate their age, gender, nationality, and their diet/lifestyle (vegan, vegetarian, flexitarian, meat-eater) to provide context to the sensory preferences recorded.

Techno-economic analysis (TEA)

Techno-economic analysis (TEA) was performed for a theoretical 200 sqm facility (Supplementary Fig. S3E). The Total Capital Investment (TCI) was computed by first assessing the Inside Battery Limit (ISBL) direct costs, which included the combined expenses of one low-temperature extruder, 3d bioprinters, vacuum filler, pneumatic fillers, bowl cutter, molds, packaging, freezing, automation, an additional 10% for missing capital and 1% for installation.

The Outside Battery Limit (OSBL) costs were calculated by summing the costs of the boiler, steam generator, chiller, and air compressor, an additional 10% addition for missing capital, and 3% for installation. The building's total cost included the production floor, laboratory, offices, workshop, warehouse, and cold storage. The Total Direct Cost (TDC) combined the ISBL and OSBL costs with the building costs. Engineering and construction were then calculated as 35% of the TDC.

The Total Plant Cost (TPC) included the TDC and engineering and construction costs. The TCI was finalized by adding 15% to the TPC for fees and contingencies. The total variable operating costs were calculated by summing the costs of all ingredients and the expenses for utilities, which included process water, power for the agitator, chiller, and facility, as well as natural gas. The Overall Equipment Effectiveness was assumed at 75%.

The 3D Printing facility was projected to accommodate four 3D printers, on the same production floor space as above. Each 3D printer with a production capacity of 6 kg/h, and twelve pneumatic fillers, based on public announcements and interviews. The 3D printing analysis predominantly utilized data on the RegenHU 3D printer[58], while for injection molding, PowerHeater (Source Technology, Denmark), operating at a capacity of 80 kg/h, was considered.

The total Operating Expense (OPEX) was calculated from the aggregation of the total costs of ingredients, utilities, and packaging for variable OPEX. The total fixed OPEX was derived from the sum of burdened labor costs, annual maintenance (including annual insurance at 4% of the TCI), and annual insurance (factored in at 5% of the TCI). Consequently, the total cost of production was determined by the addition of the total variable and fixed OPEX.

Statistical analysis

Experiments were repeated two or three times with duplicate or triplicate samples for each experimental condition unless stated otherwise. Data from representative experiments are presented, and similar trends were seen in multiple trials. A one-way ANOVA with Dunnett correction was used for calculating significant differences between groups. All error bars represent the plus standard error of the mean unless otherwise noted. One asterisk indicates $p \le 0.05$, two asterisks indicate $p \le 0.01$, and three asterisks indicate $p \le 0.001$.

Ethical approvals

Tasting trials were performed following the approval of the Hebrew University of Jerusalem Institutional Review Board (number 14032023). All participants provided written informed consent signed by the participant or legally authorized representative.

Reporting summary

Further information on research design is available in the Nature Portfolio Reporting Summary linked to this article.

Data availability

Data for the figures are provided in this paper. All data supporting the results of this study are available within the paper and its

Supplementary Information. Source data are provided in this paper. Source data are provided with this paper.

References

1. Woolston, C. Healthy people, healthy planet: the search for a sustainable global diet. *Nature* **588**, S54–S56 (2020).
2. Kozicka, M. et al. Feeding climate and biodiversity goals with novel plant-based meat and milk alternatives. *Nat. Commun.* **14**, 5316 (2023).
3. Kristiansen, S., Painter, J. & Shea, M. Animal agriculture and climate change in the US and UK elite media: volume, responsibilities, causes and solutions. *Environ. Commun.* **15**, 153–172 (2021).
4. Waglay, A., Achouri, A., Karboune, S., Zareifard, M. R. & L'Hocine, L. Pilot plant extraction of potato proteins and their structural and functional properties. *LWT* **113**, 108275 (2019).
5. Brückner-Gühmann, M., Benthin, A. & Drusch, S. Enrichment of yoghurt with oat protein fractions: structure formation, textural properties and sensory evaluation. *Food Hydrocoll.* **86**, 146–153 (2019).
6. Saldanha do Carmo, C. et al. The impact of extrusion parameters on physicochemical, nutritional and sensorial properties of expanded snacks from pea and oat fractions. *LWT* **112**, 108252 (2019).
7. Souza Filho, P. F., Andersson, D., Ferreira, J. A. & Taherzadeh, M. J. Mycoprotein: environmental impact and health aspects. *World J. Microbiol. Biotechnol.* **35**, 147 (2019).
8. Ahlborn, J. et al. Upcycling of food industry side streams by basidiomycetes for production of a vegan protein source. *Int. J. Recycl. Org. Waste Agric.* **8**, 447–455 (2019).
9. Stoffel, F. et al. Production of edible mycoprotein using agroindustrial wastes: Influence on nutritional, chemical and biological properties. *Innov. Food Sci. Emerg. Technol.* **58**, 102227 (2019).
10. Pasitka, L. et al. Spontaneous immortalization of chicken fibroblasts generates stable, high-yield cell lines for serum-free production of cultured meat. *Nat. Food* **4**, 35–50 (2023).
11. Ianovici, I., Zagury, Y., Redenski, I., Lavon, N. & Levenberg, S. 3D-printable plant protein-enriched scaffolds for cultivated meat development. *Biomaterials* **284**, 121487 (2022).
12. Saerens, W., Smetana, S., Van Campenhout, L., Lammers, V. & Heinz, V. Life cycle assessment of burger patties produced with extruded meat substitutes. *J. Clean. Prod.* **306**, 127177 (2021).
13. Bachleitner, S., Ata, Ö. & Mattanovich, D. The potential of CO2-based production cycles in biotechnology to fight the climate crisis. *Nat. Commun.* **14**, 6978 (2023).
14. De Marchi, M., Costa, A., Pozza, M., Goi, A. & Manuelian, C. L. Detailed characterization of plant-based burgers. *Sci. Rep.* **11**, 2049 (2021).
15. He, J., Evans, N. M., Liu, H. & Shao, S. A review of research on plant-based meat alternatives: driving forces, history, manufacturing, and consumer attitudes. *Compr. Rev. Food Sci. Food Saf.* **19**, 2639–2656 (2020).
16. Baune, M.-C. et al. Effect of plant protein extrudates on hybrid meatballs—changes in nutritional composition and sustainability. *Future Foods* **4**, 100081 (2021).
17. Post, M. J. Cultured beef: medical technology to produce food. *J. Sci. Food Agric.* **94**, 1039–1041 (2014).
18. Yen, F.-C. et al. Cultured meat platform developed through the structuring of edible microcarrier-derived microtissues with oleogel-based fat substitute. *Nat. Commun.* **14**, 2942 (2023).
19. Dick, A., Bhandari, B. & Prakash, S. 3D printing of meat. *Meat Sci.* **153**, 35–44 (2019).
20. Dick, A., Bhandari, B. & Prakash, S. Post-processing feasibility of composite-layer 3D printed beef. *Meat Sci.* **153**, 9–18 (2019).
21. Wilson, W. C. Jr. & Boland, T. Cell and organ printing 1: protein and cell printers. *Anat. Rec. A Discov. Mol. Cell Evol. Biol.* **272**, 491–496 (2003).
22. Dhariwala, B., Hunt, E. & Boland, T. Rapid prototyping of tissue-engineering constructs, using photopolymerizable hydrogels and stereolithography. *Tissue Eng.* **10**, 1316–1322 (2004).
23. Nahmias, Y., Schwartz, R. E., Verfaillie, C. M. & Odde, D. J. Laser-guided direct writing for three-dimensional tissue engineering. *Biotechnol. Bioeng.* **92**, 129–136 (2005).
24. Dong, H., Wang, P., Yang, Z. & Xu, X. 3D printing based on meat materials: challenges and opportunities. *Curr. Res. Food Sci.* **6**, 100423 (2023).
25. Altıparmak, S. C., Yardley, V. A., Shi, Z. & Lin, J. Extrusion-based additive manufacturing technologies: state of the art and future perspectives. *J. Manuf. Process.* **83**, 607–636 (2022).
26. Ramachandraiah, K. Potential development of sustainable 3D-printed meat analogues: a review. *Sustainability* **13**, 938 (2021).
27. Merril, A. M. *Plastics Technology*. Vol. 1 (1955).
28. Singh, G. & Verma, A. A brief review on injection moulding manufacturing process. *Mater. Today Proc.* **4**, 1423–1433 (2017).
29. Listrat, A. et al. How muscle structure and composition influence meat and flesh quality. *Sci. World J.* **2016**, 3182746 (2016).
30. Sifre, L. et al. Influence of the spatial organization of the perimysium on beef tenderness. *J. Agric Food Chem.* **53**, 8390–8399 (2005).
31. Perța-Crișan, S., Ursachi, C., Chereji, B. D., Tolan, I. & Munteanu, F. D. Food-grade oleogels: trends in analysis, characterization, and applicability. *Gels* **9**, 386 (2023).
32. Feichtinger, A. & Scholten, E. Preparation of protein oleogels: effect on structure and functionality. *Foods* **9**, 1745 (2020).
33. Prakash, S. S., Brinker, C. J., Hurd, A. J. & Rao, S. M. Silica aerogel films prepared at ambient pressure by using surface derivatization to induce reversible drying shrinkage. *Nature* **374**, 439–443 (1995).
34. Franchetti, M. & Kress, C. An economic analysis comparing the cost feasibility of replacing injection molding processes with emerging additive manufacturing techniques. *Int. J. Adv. Manuf. Technol.* **88**, https://doi.org/10.1007/s00170-016-8968-7 (2017).
35. Zielbauer, B. I., Franz, J., Viezens, B. & Vilgis, T. A. Physical aspects of meat cooking: time dependent thermal protein denaturation and water loss. *Food Biophys.* **11**, 34–42 (2016).
36. Akdogan, H. High moisture food extrusion. *Int. J. Food Sci. Technol.* **34**, 195–207 (1999).
37. Sandoval Murillo, J. L., Osen, R., Hiermaier, S. & Ganzenmüller, G. Towards understanding the mechanism of fibrous texture formation during high-moisture extrusion of meat substitutes. *J. Food Eng.* **242**, 8–20 (2019).
38. Allen Foegeding, E., Çakır, E. & Koç, H. Using dairy ingredients to alter texture of foods: Implications based on oral processing considerations. *Int. Dairy J.* **20**, 562–570 (2010).
39. Koç, H., Vinyard, C. J., Essick, G. K. & Foegeding, E. A. Food oral processing: conversion of food structure to textural perception. *Annu. Rev. Food Sci. Technol.* **4**, 237–266 (2013).
40. Stokes, J. R., Boehm, M. W. & Baier, S. K. Oral processing, texture and mouthfeel: from rheology to tribology and beyond. *Curr. Opin. Colloid Interface Sci.* **18**, 349–359 (2013).
41. Patel, A. R., Cludts, N., Sintang, M. D. B., Lesaffer, A. & Dewettinck, K. Edible oleogels based on water soluble food polymers: preparation, characterization and potential application. *Food Funct.* **5**, 2833–2841 (2014).
42. Wang, G.-S. et al. Formation of protein oleogels via capillary attraction of engineered protein particles. *Food Hydrocoll.* **133**, 107912 (2022).
43. Zhang, D. Research and overview of beyond meat's disruptive innovation. *J. Financ. Res.* **4**, 73 (2020).
44. Karagöz, İ. & Cakir Yigit, N. 27–50 (2024).
45. Souto, A., Zhang, J., Aragón, A. M., Velikov, K. P. & Coulais, C. Edible mechanical metamaterials with designed fracture for mouthfeel control. *Soft Matter* **18**, 2910–2919 (2022).

46. Douglas, T. & Stanley, G. (Special Publication (NIST SP), National Institute of Standards and Technology, 2014).
47. Atzeni, E., Iuliano, L., Minetola, P. & Salmi, A. Redesign and cost estimation of rapid manufactured plastic parts. *Rapid Prototyp. J.* **16**, 308–317 (2010).
48. Atzeni, E. & Salmi, A. Economics of additive manufacturing for end-usable metal parts. *Int. J. Adv. Manuf. Technol.* **62**, 1147–1155 (2012).
49. Yue, L., Wang, S., Wulf, V. & Willner, I. Stiffness-switchable DNA-based constitutional dynamic network hydrogels for self-healing and matrix-guided controlled chemical processes. *Nat. Commun.* **10**, 4774 (2019).
50. Baldino, N., Laitano, F., Lupi, F., Curcio, S. & Gabriele, D. Effect of HPMC and CMC on rheological behavior at different temperatures of gluten-free bread formulations based on rice and buckwheat flours. *Eur. Food Res. Technol.* **244**, https://doi.org/10.1007/s00217-018-3096-2 (2018).
51. Ghosheh, M. et al. Electro-metabolic coupling in multi-chambered vascularized human cardiac organoids. *Nat. Biomed. Eng.* https://doi.org/10.1038/s41551-023-01071-9 (2023).
52. Mortensen, L. M., Frøst, M. B., Skibsted, L. H. & Risbo, J. Effect of time and temperature on sensory properties in low-temperature long-time sous-vide cooking of beef. *J. Culin. Sci. Technol.* **10**, 75–90 (2012).
53. Fontana, A., Varith, J., Ikediala, J., Reyes, J. & Wacker, B. Thermal properties of selected foods using a dual needle heat-pulse sensor. Paper No. 996063 (American Society of Agricultural Engineers Annual Meeting, ASABE: St. Joseph, MI: Toronto, Canada, 1999).
54. Pan, Z. & Singh, R. Physical and thermal properties of ground beef during cooking. *LWT - Food Sci. Technol.* **34**, 437–444 (2001).
55. Fellows, P. J. Food Processing Technology: Principles and Practice, 3rd edn. (Woodhead Publishing, 2009). https://doi.org/10.1533/9781845696344.
56. Du, C. J., Iqbal, A. & Sun, D. W. *Computer Vision Technology for Food Quality Evaluation (Second Edition)* (ed. Da-Wen Sun) 195–212 (Academic Press, 2016).
57. Oz, F. & Zikirov, E. The effects of sous-vide cooking method on the formation of heterocyclic aromatic amines in beef chops. *LWT - Food Sci. Technol.* **64**, 120–125 (2015).
58. Balakhovsky, Y. M., Ostrovskiy, A. Y. & Khesuani, Y. D. *3D Printing and Biofabrication* (eds A. Ovsianikov, J. Yoo, & V. Mironov) 1–22 (Springer International Publishing, 2017).

Acknowledgements

Funding was provided by the Good Food Institute (GFI) grant (project no. 3011005114, Y.N.) and generous gifts from the Nikoh and the Sam and Rina Frankel Foundations (Y.N.). Mohammad Ghosheh was supported by a Neubauer Foundation Graduate Fellowship. The authors thank Prof. Itamar Willner, Prof. Daniel Cohen, Dr. Nicola Mansour, and Ilya Torchinsky for their technical guidance and support.

Author contributions

All authors read the manuscript and agree with its contents. M.G. and Y.N. conceived the hypothesis. M.G., A.E., and Y.N. designed the experiment. M.G., A.F., M.C., A.E., and Y.N. performed the experiments. M.G., L.P., and A.E. analyzed the results. M.G., A.E., and Y.N. wrote the manuscript. M.G. and Y.N. built the system. Y.N. obtained funding and supervised the project.

Competing interests

M.G. and Y.N. filed a patent application through Hebrew University. The remaining authors declare no competing interests.

Additional information

Supplementary information The online version contains supplementary material available at https://doi.org/10.1038/s41467-024-54939-y.

Correspondence and requests for materials should be addressed to Yaakov Nahmias.

Peer review information *Nature Communications* thanks Bhanu Devnani, Janam Pandya, and the other, anonymous, reviewers for their contribution to the peer review of this work. A peer review file is available.